EPJ Photovoltaics **14**, 20 (2023)

https://doi.org/10.1051/epjpv/2023011

Available online at:
www.epj-pv.org

Special Issue on 'Recent Advances in Photovoltaics 2022', edited by Mohamed Amara, Thomas Fix, Jean-Paul Kleider, Judikaël Le Rouzo and Denis Mencaraglia

REGULAR ARTICLE OPEN ACCESS

Determination of individual *I*(*V*) characteristics of each sub-cell of a triple junction device

Christophe Longeaud[1,*], José Alvarez[1], Herinirina Fanevamampiandra[1,2,3], Thomas Bidaud[2,3], Gwenaëlle Hamon[2,3], Maxime Darnon [2,3], and Marie-Estelle Gueunier-Farret[4]

[1] Laboratoire de Génie Electrique et Electronique de Paris (Geeps), CNRS, CentraleSupelec, Université Paris-Saclay, Sorbonne Université, 11 rue Joliot Curie, 91190 Gif sur Yvette, France
[2] Laboratoire Nanotechnologies Nanosystèmes (LN2) – CNRS IRL-3463, Institut Interdisciplinaire d'Innovation Technologique, Sherbrooke, Québec, Canada
[3] Institut Interdisciplinaire d'Innovation Technologique (3IT), Université de Sherbrooke, 3000 Boulevard Université, Sherbrooke, J1K 0A5 Québec, Canada
[4] Université de Bordeaux, IMS-CNRS, UMR 5218, Bordeaux INP, ENSCBP, 33405 Talence, France

Received: 3 January 2023 / Received in final form: 31 January 2023 / Accepted: 9 May 2023

Abstract. Very high conversion efficiency is reached with triple junction solar devices integrated in concentrator photovoltaic (CPV) modules. However, reduction of the active area for micro-CPV applications increases the perimeter/area ratio, enhancing losses linked to the edges. It is therefore important to characterize the perimeter influence on the final conversion efficiency. For this purpose, *I*(*V*) characterization under dark and/or light could be used as a test of the sidewalls influence. We have designed an experiment to perform *I*(*V*) curves using the light of three lasers with adjustable powers at 405, 785, and 980 nm, preferentially absorbed by the top, middle or bottom junction of the device, respectively. This experiment was applied to commercial devices made from a stack of GaInP/GaAs/Ge. In parallel we have developed a numerical calculation modeling the device to reproduce the behaviors observed during *I*(*V*) experiments. Junction parameters and influence of leakage resistances are deduced from the fit of experimental results with the numerical calculation. The *I*(*V*) experiment as well as the numerical calculation are presented in details. It is also underlined that, combining both experiment and calculation, the *I*(*V*) characteristic of each junction as if it was isolated can be determined.

Keywords: Triple junction device / Sub-cell I-V characteristics / Leakage resistances / Open-circuit voltage / Short-circuit current

1 Introduction

High efficiency solar cells and modules are obtained with multi-junction (MJ) solar cells, with record efficiencies of 47.6% under 665× concentration [1]. Today's commercial cells in Concentrated Photovoltaics (CPV) modules have a size around 3×3 mm^2 and are integrated in modules equipped with Fresnel lens panels [2]. However, many reasons push towards the miniaturization of these cells such as an improved heat management and/or reduced resistance losses and many teams and researchers are pushing towards micro-CPV [3–6]. Yet, due to the reduction in their size, the impact of perimeter losses will be amplified [7,8]. The influence of the perimeter on the device performances results in voltage losses due to recombination of minority carriers at the edges of the device. Passivation techniques have been used in Sherbrooke University to reduce the impact of edges on the electrical characteristics [9], but V_{OC} losses are still remaining. To keep on the miniaturization pathway, assessment of the surface passivation is required. Indeed, no characterization technique succeeded in estimating which sub-cell suffers the most of the size reduction. This quantification is made complex due to the fact that sub-cells are serially interconnected [10,11]. Thus, it would be of high value to develop a characterization technique that allows to characterize each sub-cell independently.

I(*V*) measurements of MJ devices based on different light and voltage biases were proposed and detailed in the 1980 s by Burdick and Glatfelter [12] and applied to amorphous silicon tandem cells. Since then, this technique of light and voltage biasing was largely used in the study of triple junction devices [13]. Besides, Fafard et al. recently

* e-mail: christophe.longeaud@geeps.centralesupelec.fr

proposed a method, based on $I(V)$ measurements under different intensities of light biases, to investigate the quality of triple junction solar cells [14]. Still, these methods suffer from the presence of artefacts during measurements. Several methods were proposed to minimize or even correct these artefacts [15,16]. Isotype devices, in which two junctions are short-circuited to reveal the third one, have been employed to avoid measurements artefacts, but these devices are far from the real devices where all the junctions are interdependent.

To our knowledge none of the techniques proposed so far can bring enough information on each individual cell to eventually allow to derive the $I(V)$ characteristic of each one as if it was isolated.

In this work we present a methodology that we have developed which, combined with a numerical calculation, can lead to the determination of $I(V)$ characteristics of each individual junction as if it was isolated. Our method is based on the measurements of $I(V)$ curves under a light bias imposed by three different lasers instead of color filtered light or LEDs approaches [14,17]. These three lasers can be used individually to illuminate preferentially one junction under various powers, or combined to illuminate two or even three of the junctions.

The associated numerical simulation of triple junction devices to reproduce the experimental results will be presented. Combining the experimental results and the fits from the numerical simulation we were able to propose a complete model of the studied triple junction device.

This article details this measurement method and its associated model, applied on a commercial triple-junction solar cell. A successful fit of the $I(V)$ curves is obtained and we can decorrelate electrical parameters of each cell on an individual basis.

2 Samples and experiment

2.1 Samples

The studied triple junction devices are two-terminal GaInP/GaInAs/Ge commercial solar cells with an active cell area of 3×3 mm^2 and a rated efficiency of 43.7% at 250 suns. The cells were soldered and wirebonded on a receiver at Université de Sherbrooke. Figure 1 gives a schematic of one of the solar cells and its External Quantum Efficiency (EQE) measured using our QEX7 system from PV measurements. The dashed vertical lines indicate the wavelengths of the biases of laser light used in this work.

Two samples of the same batch were studied both experimentally and numerically. The experimental results presented the same trends and behaviors for both samples, thus, to illustrate our method, we only detail the results for one of them in the following.

2.2 Experiment

The experimental setup is a probe station with external light sources for light-biasing the device under test (DUT). We use three lasers emitting at 405 nm, 785 nm, 980 nm, each of them with power emission up to 180 mW as light

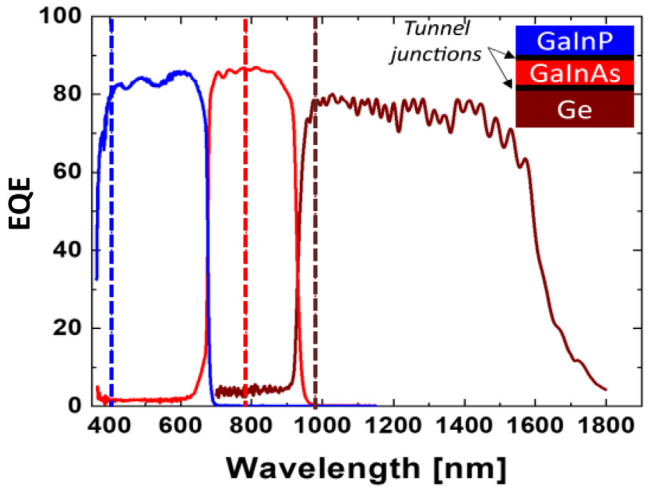

Fig. 1. EQE of the triple junction solar cells investigated here. The inset shows a schematic view of the arrangement of the sub-cells.

sources. They provide light biases to illuminate preferentially one junction or the other. On triple junction solar cells, these three wavelengths are used to illuminate mainly the top cell, middle cell and bottom cell, respectively. The light coming out of the laser at 405 nm is injected into an optical fiber at the output of which a lens is set to focus the light into the entrance of a fiber bundle after reflection onto a dichroic mirror. The two lasers at 785 and 980 nm are coupled so the light coming out of each of the lasers is injected into the same optical fiber. A lens is fixed at the output of this fiber to focus the light into the entrance of the fiber bundle. Figure 2 describes schematically the system used to drive the laser lights into the fiber bundle.

The DUT is fixed in front of the output of the fiber bundle ($\phi \approx 5.5$ mm) so that it can be enlightened with any of the chosen wavelengths. The distance between the output of the fiber bundle and the sample (~5 mm) is set so that the whole area of the device is enlightened. The powers delivered by the lasers are adjustable. The power at the output of the fiber bundle is between 15% and 24% of the power at the output of the lasers (15% for 405 nm, 24% for 785 nm and 16% for 980 nm). In the following the powers given in the text are those at the output of the lasers. Hence, when a power of 20 mW is given it means that the actual power at the output of the fiber bundle is 3 mW at 405 nm, 4.8 mW at 785 nm and 3.2 mW at 985 nm. Except for light-biasing, the DUT is maintained in the dark so that no parasitic light can trouble the results.

Therefore, we can illuminate the device with wavelengths adapted to one, two or three chosen sub-cells at a given power and, subsequently, measure $I(V)$ variations under fixed illumination conditions. The idea is to use the results of these experiments to deduce as many parameters of the junctions as possible (short-circuit current, V_{OC}, shunt resistance...). To measure the $I(V)$ curves we use a current/voltage converter (SR570 from Stanford Research) with which the voltage applied to the device can vary in the range [–5 V, +5 V]. In these experiments, we use here a range of [0 V, 2.5 V]. An in-house program allows

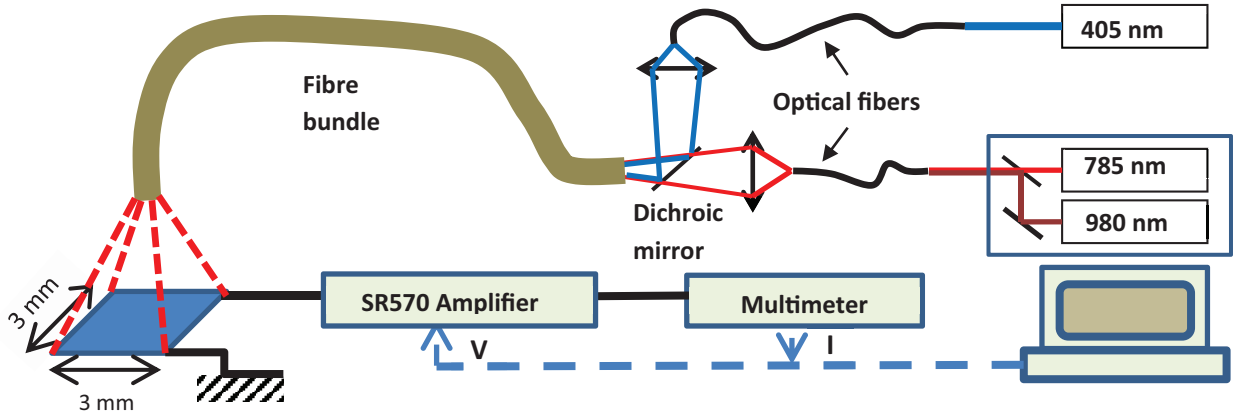

Fig. 2. System developed to illuminate a device with three different wavelengths. The light coming from three different lasers is injected into a fiber bundle at the other end of which the device is positioned.

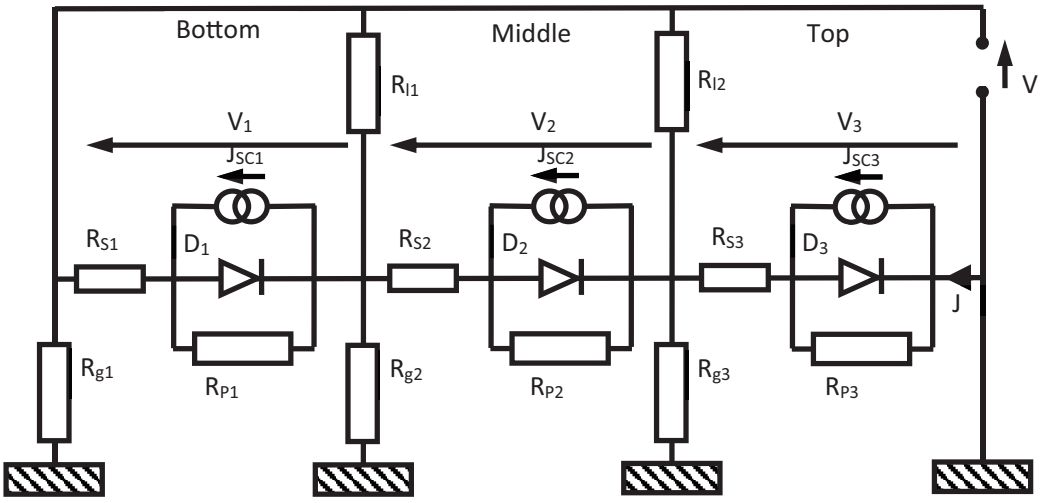

Fig. 3. Model of a triple junction introduced in a numerical calculation to reproduce the experimental measurements.

to control the SR570 (applied voltage and gain) and reads the output voltage on an Agilent 3440 to automatically obtain the evolution of the current flowing through the device with respect to the applied voltage, thus the $I(V)$ curve.

To study the efficiency of the device we have illuminated the cell with an AM1.5G spectrum delivered by an Oriel Instruments solar simulator to determine its $J(V)$ characteristics.

2.3 Numerical calculation

We developed a numerical calculation to reproduce the $I(V)$ characteristics that have been experimentally measured [18]. The model is described in Figure 3. To reduce the number of parameters for the fitting of the experimental results we used a one diode model for each junction. Each junction i is characterized by its short circuit current J_{sci}, its diode D_i, its parallel resistance R_{Pi} and its series resistance R_{Si}.

To model possible shunt resistances originating from the edges of the device, we have added leakage resistances to the standard model of a triple junction device. These resistances are connected both toward the ground (R_{gi} for junction i) and toward the high voltage terminal (R_{li} for junction i) of the device. It can be seen that the leakage resistances R_{l1} and R_{g3} are in parallel with $R_1 = R_{p1} + R_{s1}$ and $R_3 = R_{p3} + R_{s3}$, respectively. Therefore, they may be difficult to estimate for their influence may lead to estimated values of R_1 or R_3 lower than their actual values. This model is a simplified approach of the different shunt types that can be found in solar cells since, for instance, several shunt types were found in crystalline silicon, some of them presenting rectifying properties [19].

We have also simplified the connections between the cells replacing the tunnel junctions by single series resistances. Indeed, taking account of the current densities used in our experiments we can assume that the tunnel junctions are working in the ohmic part of their $I(V)$ characteristics [20].

The calculations are performed by solving the following equation, equation (1), for each junction, the sign conventions for J and V_i being those shown in Figure 3

$$J = J_{sci} - J_{sdi} * \left[Exp\left(\frac{V_i + R_{si}J}{m_i k_b T}\right) - 1\right] - \left(\frac{V_i + R_{si}J}{R_{pi}}\right). \quad (1)$$

J_{sdi} is the saturation currents and m_i the ideality factor of the diode D_i, k_b is the Boltzmann constant and T is the temperature. The calculations are done at $T = 300$ K.

Once the parameters of each junction are defined, it is possible to calculate and plot the $J(V)$ curves of the device when all the junctions are illuminated, when only two junctions are illuminated or when only one junction is illuminated taking into account, or not, the leakage resistances. It is also possible to calculate the $J(V)$ curves of each junction taken separately under the same conditions of illumination. The conditions of illumination are fixed by the choice of the short circuit current densities J_{sci}, i being the index of the junction.

For the calculation for each junction separately equation (1) is solved for J at fixed values of V. For the calculations performed on the whole device equation (1) is solved for V for given values of J. The J steps are adjusted as function of the variations of V. A small (large) variation of V is compensated by a large (small) variation of J.

With a rapid look at Figure 3 it is easy to understand that, despite the simplifications we have introduced, a very large number of parameters have to be dealt with. Thus, it is mandatory to extract as many parameter estimates as possible from the experimental data to end with a 'reliable' set of parameters describing the device and its behavior.

3 Results and discussion

3.1 Experimental results

Figure 4 presents $I(V)$ curves, and their fits, measured under different light biases for each sub-cell. Figure 4a presents the $I(V)$ curves while the middle cell or the middle and the bottom cells are illuminated, therefore probing the influence of the top cell. Figure 4b presents the $I(V)$ curves while the top cell or the top and the bottom cells are illuminated, therefore probing the middle cell. Figure 4c presents the $I(V)$ curves while the top cell or the top and the middle cells are illuminated, therefore probing the bottom cell. The symbols represent the experimental data and the lines the fits with the numerical calculation.

Figure 4a shows that when illuminating the device at 785 nm with an output power of 20 mW the current at 0 V is in the order of 400 pA. This value remains the same when a 980 nm illumination of 20 mW is added. However, we can see that if one adds an illumination at 405 nm (Fig. 4c) with a power of 20 mW, $I(0)$ rises at ~350 μA. Thus we can assume that for a power of 20 mW (Fig. 4c, curve illustrated as 20 mW All or dark yellow filled diamonds 20 mW at 785 nm and 20 mW at 405 nm) the current of 350 μA is the current generated by the top junction. Note that for a given illumination power at 405 nm, the short-circuit current of the top cell varies linearly with the sum of the laser powers at 785 and 980 nm before reaching a saturation value. The same behavior takes place when looking at the middle cell as illustrated in Figure 5. Indeed when illuminating at 785 nm with a power of 20 mW, if one fixes the power at 980 nm at 5 mW and increases the 405 nm laser power the current follows linearly the increase until the output power of the 405 nm laser reaches 80 mW. Above this value the current starts to saturate to reach a final value of 1.85 mA. Thus, we can reasonably assume that, under these conditions (20 mW at 785 nm, 80 mW at 405 nm, 5 mW at 980 nm at the laser outputs), the current is limited by the middle cell and that the short-circuit current of the middle junction when illuminated at 785 nm with a power of 20 mW is $I_{\mathrm{SCmiddle}} \approx 1.85$ mA. We have to underline that the power of the laser at 980 mW has almost no influence on this value found the same with $P(980) = 20$ mW.

Once the short circuit current of the middle junction is estimated, keeping the powers of the other lasers at the values fixed for this estimate ($P(980) + P(405) \geq 85$ mW), it is possible to estimate the value of the ideality factor of the middle junction by playing with the power at 785 nm and plotting the variation of the open-circuit voltage *vs* the short-circuit current for different values of the power of the light sent to the limiting junction. From a semi-logarithm plot one can deduce the ideality factor as was done by S. Fafard and co-workers [14]. As shown in Figure 6, in the present case we have found an ideality factor of $m \approx 1.6$ for the middle junction.

The same analysis can be done for the top cell when one illuminates the device with the 405 nm laser with a power of 20 mW. Figure 4b shows that the current $I(0)$ using only the illumination at 405 nm with a power of 20 mW is low, of the order of $I(0) \approx 0.35$ μA. This current increases up to 9.7 μA if an illumination at 980 nm with 20 mW is superimposed (Fig. 4b). If an illumination at 785 nm is superimposed with a power of 2 mW (Fig. 4c) the current increases up to 228 μA. If the power of the 785 nm laser is increased again $I(0)$ continues to rise until it reaches a value of the order of 350 μA and stays constant whatever the output powers of the 785 nm and 980 nm lasers. Hence, we can assume that the short-circuit current of the top junction illuminated at 405 nm with a power of 20 mW is $I_{\mathrm{SCtop}} \approx 350$ μA.

Once the top junction is set as the limiting junction, it is again possible to plot the variation of the open-circuit voltage *vs* the short-circuit current for different values of the power of the light at 405 nm sent to it. From a semi-logarithm plot we have deduced $m \approx 2.1$ for the top junction. This value, of the order of 2 can be surprising but we may stress that such a value was already measured for III-V solar cells [21]. Besides, values even larger than 3 have been found in damaged c-Si wafers [22].

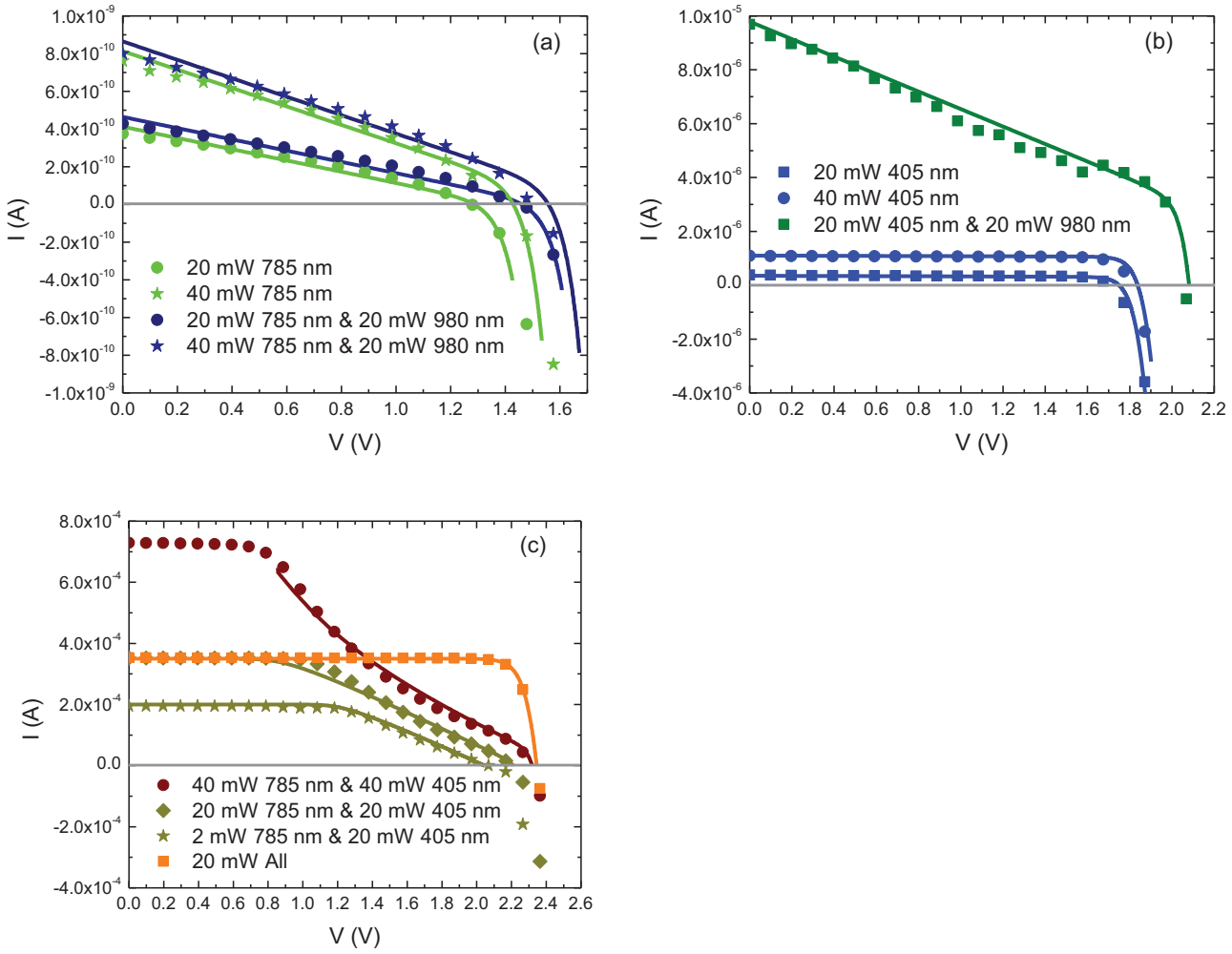

Fig. 4. $I(V)$ experimental results (symbols) obtained on our sample. The power at the output of the lasers used for the experiment is displayed in the figure. The lines are the fits obtained with the numerical simulation.

Unfortunately, it was not possible to determine the short circuit current of the bottom junction which seems to be always larger than the I_{SC} of the two other junctions even with very low power of the 980 nm laser. For the numerical calculation we have assumed a value of $I_{SCbottom}$ of 2 mA for an illumination at 20 mW of the laser at 980 nm but it is probable that this value is underestimated. We have also chosen to take an ideality factor $m = 1$ for the bottom junction [23].

As mentioned above, when only one junction, top or middle, is illuminated the current at 0 V is extremely low. The reason is that it is limited by the resistances in series induced by the shunt resistances of the other junctions assumed to be under dark. An order of magnitude of these resistance in series can be deduced by the slopes of the $I(V)$ curves when the voltage varies in the range [0 V, 1 V]. When illuminating only the middle junction an order of magnitude of the resistance in series is $R_{Smiddle} \approx 3.5$–4 GΩ (see Fig. 4a, 20 mW at 785 nm). When illuminating only the top junction, from the results presented in Figure 4b one can find an order of magnitude of the resistance in series: $R_{Stop} \approx 45$ MΩ. Theoretically, assuming that the series resistances of each junction is low, these resistances in series are the sum of the parallel resistances of the junctions under dark: $R_{Smiddle} = R_{Ptop} + R_{Pbottom}$ and $R_{Stop} = R_{Pmiddle} + R_{Pbottom}$. An estimate of the parallel resistance of the bottom junction can be obtained if one illuminates the device with two wavelengths absorbed by the top and middle junctions, 405 nm and 785 nm respectively. Considering the results presented in Figure 4c at low output power (20 mW at 405 nm and 2 mW at 785 nm) it can be seen that the current is almost constant at low voltages and then decreases almost linearly when increasing the voltage before decreasing exponentially for high voltages. From the linear decrease of the current one can deduce that the resistance limiting the current is $R_{Pbottom} \approx 3.5$ kΩ.

Up to this point, with simple considerations on an ideal triple junction device, we have deduced the ideality factors and short-circuit currents for the top and middle junctions when illuminated with the appropriate laser at a power of 20 mW. We have also estimated the parallel resistances of each junction assuming that their series resistances were negligible. The challenge is that we are not dealing neither with an ideal experiment nor with an ideal device.

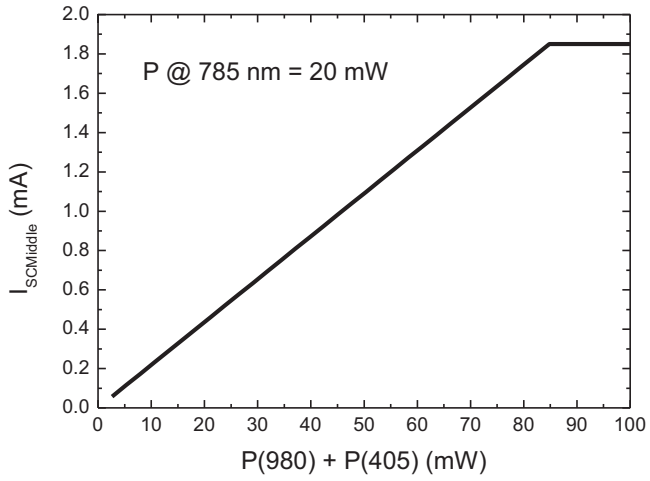

Fig. 5. Evolution of the short-circuit current I_{SC} measured when increasing the illumination of the top and bottom cells up to 100 mW. I_{SC} saturates at 1.85 mA.

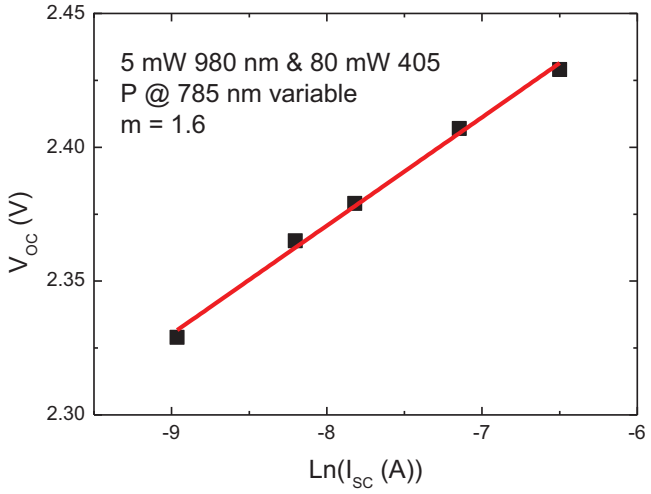

Fig. 6. Estimate of the ideality factor of the middle junction by playing with the power of the illumination at 785 nm.

3.2 An ideal experiment?

Concerning the experiment one would assume that when using a single laser only the junction the most sensitive to the laser wavelength is illuminated, the two others being in the dark. Considering our results it is certainly not the case. Indeed, it can be seen in Figure 4a that an illumination at 785 nm with a power of 20 mW leads to an open circuit voltage of $V_{OC} = 1.3$ V, a value much larger than expected for the middle junction. In addition, it can be seen in Figure 4b that an illumination at 405 nm with a power of 20 mW leads to an open circuit voltage of $V_{OC} = 1.7$ V, a value also much larger than expected for the top junction. A simple addition shows that with the combination of these two illuminations we should obtain $V_{OC} = 3$ V, a value which, besides being completely unrealistic, is much higher than the 2.2 V we found (see Fig. 4c, 20 mW at 785 and 405 nm).

Note that when an illumination of 20 mW with the laser at 980 nm is added to an illumination with 20 mW at 785 nm (Fig. 4a) or to both illuminations with 20 mW at 405 nm and 785 nm (Fig. 4c) the V_{OC} increases by ~0.16 V, a value which, associated with our estimation of the $I_{SCbottom}$, gives a basis for fixing the value of the parameters of the diode introduced in the simulation to model the bottom junction.

Whatsoever, if we add these 0.16 V to the measured V_{OC} when each junction is illuminated with a single laser, we should end up with a V_{OC} of 3.16 V when all the junctions are illuminated with a power of 20 mW whereas, we measure $V_{OC} = 2.35$ eV (see Fig. 4c, all junctions illuminated). We have thus assumed that the sum of the $V_{OCtop} + V_{OCmiddle}$ should be of the order of 2–2.3 V, with $1.1\text{ V} \leq V_{OCtop} \leq 1.3\text{ V}$ and $0.85\text{ V} \leq V_{OCmiddle} \leq 1\text{ V}$, and sought an explanation for the discrepancy between the expected V_{OC} and the measured ones.

With the simulation, it can be shown that if one chooses the diode parameters of the middle junction so as to have $V_{OCmiddle} = 1$ V with $I_{SCmiddle} = 1.8$ mA, then a small current of 0.4 µA (4500 times lower) will generate a $V_{OCmiddle}$ of 0.4 V. Hence, when one illuminates the top junction, if it generates a current in the middle junction (even a very small one), the total V_{OC} will be largely higher than the V_{OC} of the top junction alone. The origin of this small current can be attributed to an incomplete absorption of the 405 nm light by the top cell or to photoluminescence from the top cell which in turn induces a current in the middle junction. A last option is that the laser itself generates a very small contribution at another wavelength than 405 nm that reaches the middle junction and generates a small current in it. However, if we introduce at the output of the laser a blue filter with a band pass between 350 and 600 nm we do not observe any modification of the results. Thus, this last option has to be rejected leaving only the first two assumptions as an explanation for the small current generated in the middle junction when the top junction is illuminated.

Still with the simulation, it can be shown that if one chooses the diode parameters of the top junction so as to have $V_{OCtop} = 1.15$ V with $I_{SCtop} = 350$ µA, then a very small current of $I_{SCtop} = 400$ pA, ~10^6 times lower, will generate a V_{OCtop} of 0.4 V. Again, when one illuminates the middle junction and if the top junction generates a very small current then the total V_{OC} will be largely higher than the V_{OC} of the middle junction alone. The origin of this current is more difficult to explain than in the previous case. Indeed, the gap of the top junction is of the order of 1.86 eV and the photon energy at 785 nm is 1.58 eV so the light should go through the top junction without generating any carriers with an ideal semiconductor. Could this generation come from deep states with a density 10^6 times lower than the band edge density? This is an open question, the presence of defects at such a low concentration being rather tricky to put into evidence. Generation in the top junction by the luminescence of the middle junction seems also highly improbable, though optical coupling of the bottom sub-cell with the top sub-cell of an MJ device has

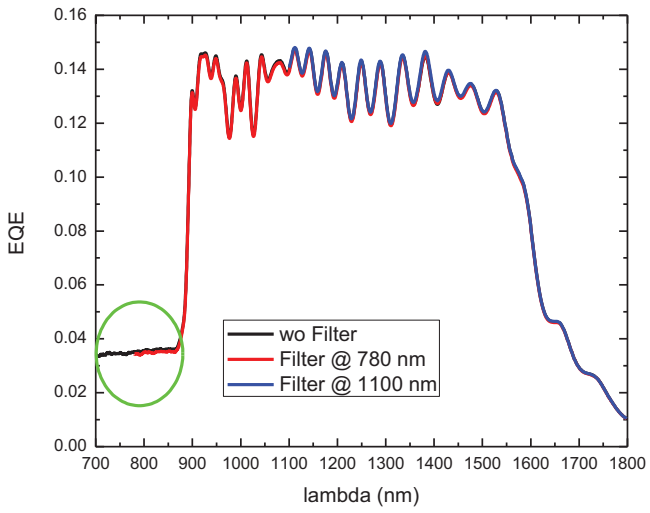

Fig. 7. EQE response of an isotype cell where only the bottom junction is active. In the regions where they can be measured the responses are the same independently of the used filters. The green circle indicates a contribution of the Ge cell even in the region where the light is assumed to be absorbed by the cells above.

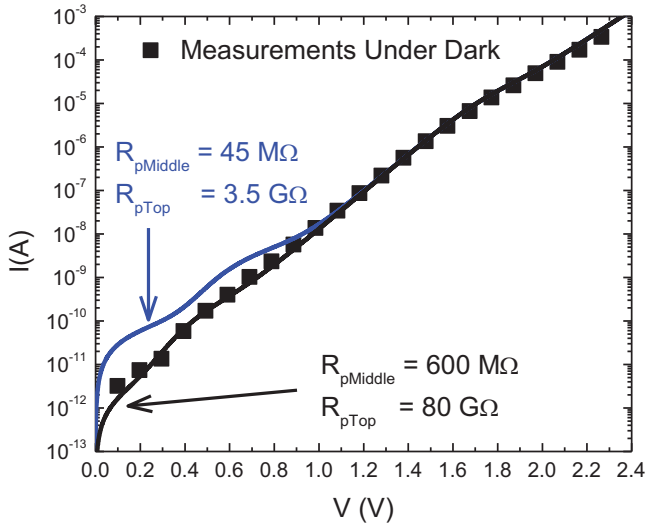

Fig. 8. $I(V)$ curves under dark for our sample. Experimental results (symbol) are fitted (lines) by the results of the calculation with numerical simulations including different parameters. The arrows indicate the influences of R_{Ptop} and R_{Pmiddle} on the shape of the fitting curve.

been already reported [17]. The last option in which the laser generates a small contribution at a lower wavelength than 785 nm is still possible though we have added a high pass filter to suppress the wavelengths shorter than 750 nm at the output of the 785 nm laser to suppress any parasitic contribution of the laser.

Finally, it is worth noticing that the bottom cell may be illuminated through the middle one when one uses a laser at 785 nm. This is demonstrated in Figure 7 which shows the Ge response of an isotype cell in which the top (InGaP) and middle (GaAs) "sub-cells" were n-type only (no junction). It can be seen (in the green circle) that the Ge cell is responding even at wavelengths supposed to be absorbed by the middle cell on top of it. This response in the range 700–850 nm is not an artifact coming from the response of the middle junction [13], artifact which is not expected in an isotype device. This response of the bottom cell to 785 nm illumination is likely due either to light transmission or photoluminescence of the InGaAs on top of the bottom cell, because the response of the Ge junction remains the same even if we add high pass filters at 780 nm or at 1100 nm for which the contribution of the middle junction would be largely minimized.

The response of the Ge junction when the middle cell is illuminated was taken into account in the numerical calculation to fit the experimental results.

In conclusion, we cannot assume that when illuminating mainly one junction with the appropriate laser only the targeted junction contributes to the $I(V)$ curve. There is always a small contribution of the other two junctions, each contribution depending on the wavelength of the illuminating laser, and these contributions have to be taken into account in the simulation.

3.3 An ideal device?

An ideal device would be the one described in Figure 3 with infinite leakage resistances ($R_{g1} = R_{g2} = R_{g3} = R_{l1} = R_{l2} = \infty$) but experimental results contradict this possibility.

First, a close look at the curves in Figure 4a reveals that the resistance in series is not the same when working with a laser at 785 nm with 20 mW power or with 40 mW power: with 20 mW the resistance in series is 3.5 GΩ and with 40 mW the resistance in series is 2.1 GΩ.

Another problem can be seen when performing measurements with the 405 nm laser (Fig. 4b). If only this laser is used the resistance in series is ∼ 45 MΩ whatever the power, but if one adds a laser at 980 nm with a power of 20 mW this resistance in series drops down to 310 kΩ.

Besides, when dealing with the illumination of the top and middle junctions (Fig. 4c) it can be seen that at low power (2 mW for the laser at 785 nm), one can deduce a resistance in series of ∼ 3.5 kΩ, value that was chosen for the shunt resistance of the bottom cell. But with higher powers the curve presents a strange shape that cannot be fitted with a single resistance in series.

Finally, using the parallel resistance values found from experiments performed under light, we have tried without success to reproduce the results obtained under dark. This is presented in Figure 8.

Clearly, the model for the triple junction proposed in Figure 3 is not completely appropriate to reproduce all the experimental results. However, it can be seen in Figure 4 that the model seems to be sufficient to calculate curves fitting the experimental data obtained at several powers and wavelengths of illumination. For this purpose we have made the following assumption: the resistances obtained under light from the results presented in Figure 4 are linked

to defects at the edges of the device which contribution depends on the intensity and wavelength of the illumination.

Indeed, in Figure 8 it is possible to obtain a good fit of the $I(V)$ curve under dark assuming that $R_{\mathrm{Ptop}} = 80$ GΩ and $R_{\mathrm{Pmiddle}} = 600$ MΩ (black line) instead of $R_{\mathrm{Ptop}} = 3.5$ GΩ and $R_{\mathrm{Pmiddle}} = 45$ MΩ (blue line). Based on this assumption we have introduced the proper parallel resistances for each junction and tried to play with the leakage resistances to match the experimental results.

In the case of illumination with the laser at 785 nm at 20 mW (Fig. 4a), we have introduced a leakage resistance $R_{\mathrm{g1}} = 3.5$ GΩ and with a power of 40 mW at 785 nm we have chosen $R_{\mathrm{g1}} = 2.1$ GΩ.

With an illumination at 405 nm (Fig. 4b), we have introduced a leakage resistance $R_{\mathrm{g2}} = 45$ MΩ and when superimposing an illumination of 20 mW at 980 nm we have introduced a leakage resistance $R_{\mathrm{l2}} = 310$ kΩ without changing the junction parameters to calculate the $I(V)$ curve.

Finally, for the last case, measurements with 40 mW at 405 and 785 nm, we have defined a parallel resistance of the bottom cell varying with the applied voltage as $3100\ V^2/(V^2+1)+900$ Ω. This expression is ***only phenomenological*** and has absolutely no physical justification except the fact that between 1 V and 1.4 V the resistance in series that can be extracted from the curve is of the order of 2 kΩ whereas in the range 1.6–2 V the resistance in series is of the order of 3.2 kΩ. With the above expression, the resistance in series, which would be the parallel resistance of the bottom cell, varies between 900 Ω (0 V) and 3500 Ω (2.2 V) and the final fit matches quite well with the experimental data. Since this approach is phenomenological, we may assume that any function presenting similar variations of the resistance *vs* voltage (some sort of crank handle shape) would be appropriate for a fitting of the curve. In addition, we cannot reject the fact the resistance we measure is actually a shunt resistance in parallel with the parallel resistance of the bottom cell or simply reflects the behavior of the tunnel junction.

The data introduced in the numerical calculation is presented in Table A1 in the Appendix A of this document.

One can wonder about the origin of these leakage resistances and for the moment the only explanation that comes in mind is the influence of the edges which, because of the defects, could be the cause of the evolution, with or without light, of the 'parallel' resistances of the considered junctions. Up to this point, we cannot definitely conclude on the ohmicity or rectifying properties of the defects introducing shunts that we have put into evidence.

Nevertheless, though as a matter of simplification, to avoid an accumulation of fitting parameters and very complex calculations, we have modeled their behaviors by leakage resistances, the fact that the values of these leakage resistances depend on the wavelength and power of the illumination (Fig. 4a), as well as on the applied voltage (Fig. 4c), suggests that we are more probably dealing with rectifying shunts.

Finally, the reader may note that, since we have determined some of the parameters of the junctions, it is theoretically possible to plot the $J(V)$ curves of each junction under AM1.5G as if it was considered alone. For this purpose, we have introduced the values of the current densities we should obtain under AM1.5G that we have deduced from EQE measurements performed on the device (see Fig. 1). The results of the calculation are presented in Figure 9a. It is also possible to predict the $J(V)$ curve shape under AM1.5G and to compare with the experimental results. This is shown in Figure 9b where we end with an excellent agreement between all the parameters (J_{SC}, V_{OC}, and FF). So far, though rather simple, it seems that the model we have defined gives a good overview of the device properties.

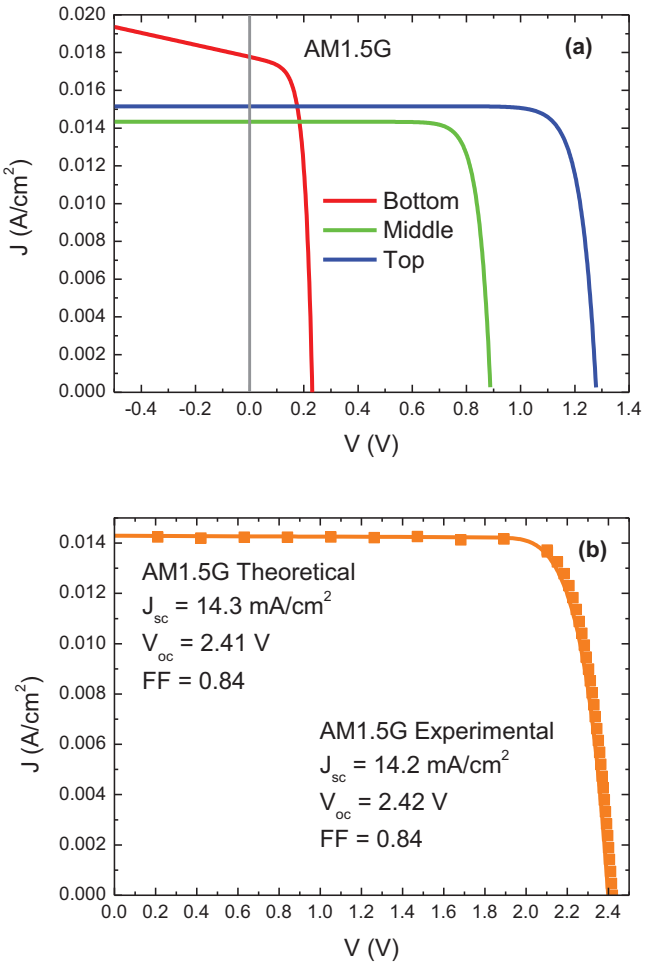

Fig. 9. (a) $J(V)$ characteristics of each junction taken alone under AM1.5G, (b) comparison of the experimental (squares) and theoretical (line) $J(V)$ characteristics of the device under AM1.5G.

4 Conclusion

We have shown that $I(V)$ measurements performed with lasers of different wavelengths with several powers and superimposition of their emissions can bring some information on the properties of triple junction photovoltaic devices. Many parameters, such as short-circuit currents and ideality factors could be deduced directly

from the experimental results. Nevertheless, to lead to a complete overview of the device parameter, these experimental results had to be combined with numerical calculations to derive each junction parameters and put into evidence the influence of defects generating shunts at the edge of the device.

For instance, we have shown that though we had chosen wavelengths to be absorbed by each of the junction, 405 nm for the top, 785 nm for the middle and 980 nm for the bottom, we always had a small contribution of at least one adjacent junction resulting in V_{OC} values much higher than expected. We have also shown that resistances deduced from the experiment were linked to leakage resistances probably coming from defects located at the edge of the device and shunting the junctions.

We could not conclude on the nature of these shunts (rectifying or ohmic) because we had to simplify our model to limit the number of adjustable parameters and the complexity of the calculation. Yet, the fact that the values of the leakage resistances depend on the wavelength and power of the illumination, as well as on the applied voltage, suggests that some of these shunts are rectifying.

Despite the simplicity of our model, we were able to define a complete set of parameters with which all the experimental results were reproduced. Besides, we could define the $J(V)$ curves under AM1.5G for each junction taken individually and reproduce the $J(V)$ characteristics of the complete device under AM1.5G.

The next step will be to study several devices which edges have been treated differently to compare both the set of parameters that can be deduced from experiment and calculation, and their conversion efficiencies to eventually optimize the technological process of microcell fabrication.

Appendix A: Table A1

When $I_{sc} = 0$ is indicated it means that this junction was not taken into account in the calculation.

'Variable' means that R_{p1} varies as $R_{p1} = 3100\ V^2/(V^2+1)+900$ (phenomenological).

The values of the leakage resistances are in bold characters.

R_{l1} and R_{g3} were always fixed at very high values.

For the fitting of the $I(V)$ curves applying only 20 mW and 40 mW at 785 nm we have assumed that the I_{sc} of the bottom cell were 20 µA and 40 µA, respectively, to take into account that the light at 785 nm is not fully absorbed by the cells above the Ge junction.

Appendix B: Results obtained on the second sample

Figure B1 displays the results obtained with different lasers with different powers illuminating the sample. The general behaviors are the same as those observed with the sample described in the main text of this communication (see Fig. 4).

With the parameters deduced from the combined experiment and simulation performed on the sample #2, we were also able to plot the $I(V)$ curves of each junction as if it was isolated (Fig. B2a) and to fit the $I(V)$ curve of the complete device measured under AM1.5G (Fig. B2b).

Table A1. Parameters for fitting the experimental $I(V)$ data of our MJ cell.

Param.	20 mW 785 and 20 mW 980	40 mW 785 and 20 mW 980	20 mW 405	40 mW 405	20 mW 405 and 20 mW 980	20 mW 405 and 20 mW 785	40 mW 405 and 40 mW 785	20 mW All
R_{s1} (Ω)	1	1	1	1	1	1	1	1
R_{p1} (Ω)	3.5×10^3	3.5×10^3	3.5×10^3	3.5×10^3	3.5×10^3	3.5×10^3	Variable	3.5×10^3
I_{sc1} (A)	2.0×10^{-3}	2.0×10^{-3}	0	0	2.0×10^{-3}	4.0×10^{-5}	9.0×10^{-5}	2.0×10^{-3}
I_{sd1}(A)	2.0×10^{-7}	2.0×10^{-7}	2.0×10^{-7}	2.0×10^{-7}	2.0×10^{-7}	2.0×10^{-7}	2.0×10^{-7}	2.0×10^{-7}
m_1	1	1	1	1	1	1	1	1
R_{s2} (Ω)	1	1	1	1	1	1	1	1
R_{p2} (Ω)	6.0×10^8	6.0×10^8	6.0×10^8	6.0×10^8	6.0×10^8	6.0×10^8	6.0×10^8	6.0×10^8
I_{sc2} (A)	1.8×10^{-3}	3.6×10^{-3}	3.5×10^{-7}	1.1×10^{-6}	5.9×10^{-6}	1.8×10^{-3}	3.6×10^{-3}	1.8×10^{-3}
I_{sd2} (A)	6.0×10^{-13}	6.0×10^{-13}	6.0×10^{-13}	6.0×10^{-13}	6.0×10^{-13}	6.0×10^{-13}	6.0×10^{-13}	6.0×10^{-13}
m_2	1.6	1.6	1.6	1.6	1.6	1.6	1.6	1.6
R_{s3} (Ω)	1	1	1	1	1	1	1	1
R_{p3} (Ω)	8.0×10^{10}	8.0×10^{10}	8.0×10^{10}	8.0×10^{10}	8.0×10^{10}	8.0×10^{10}	8.0×10^{10}	8.0×10^{10}
I_{sc3} (A)	4.5×10^{-10}	8.5×10^{-10}	3.5×10^{-4}	7.0×10^{-4}	3.5×10^{-4}	3.5×10^{-4}	7.3×10^{-4}	3.5×10^{-4}
I_{sd3} (A)	8.0×10^{-14}	8.0×10^{-14}	8.0×10^{-14}	8.0×10^{-14}	8.0×10^{-14}	8.0×10^{-14}	8.0×10^{-14}	8.0×10^{-14}
m_3	2.1	2.1	2.1	2.1	2.1	2.1	2.1	2.1
R_{l2} (Ω)	1.0×10^{13}	1.0×10^{13}	1.0×10^{13}	1.0×10^{13}	$\mathbf{3.1 \times 10^5}$	1.0×10^{13}	1.0×10^{13}	$\mathbf{3.1 \times 10^5}$
R_{g1} (Ω)	$\mathbf{3.5 \times 10^9}$	$\mathbf{2.1 \times 10^9}$	1.0×10^{13}	1.0×10^{13}	1.0×10^{13}	$\mathbf{3.5 \times 10^9}$	$\mathbf{2.1 \times 10^9}$	$\mathbf{3.5 \times 10^9}$

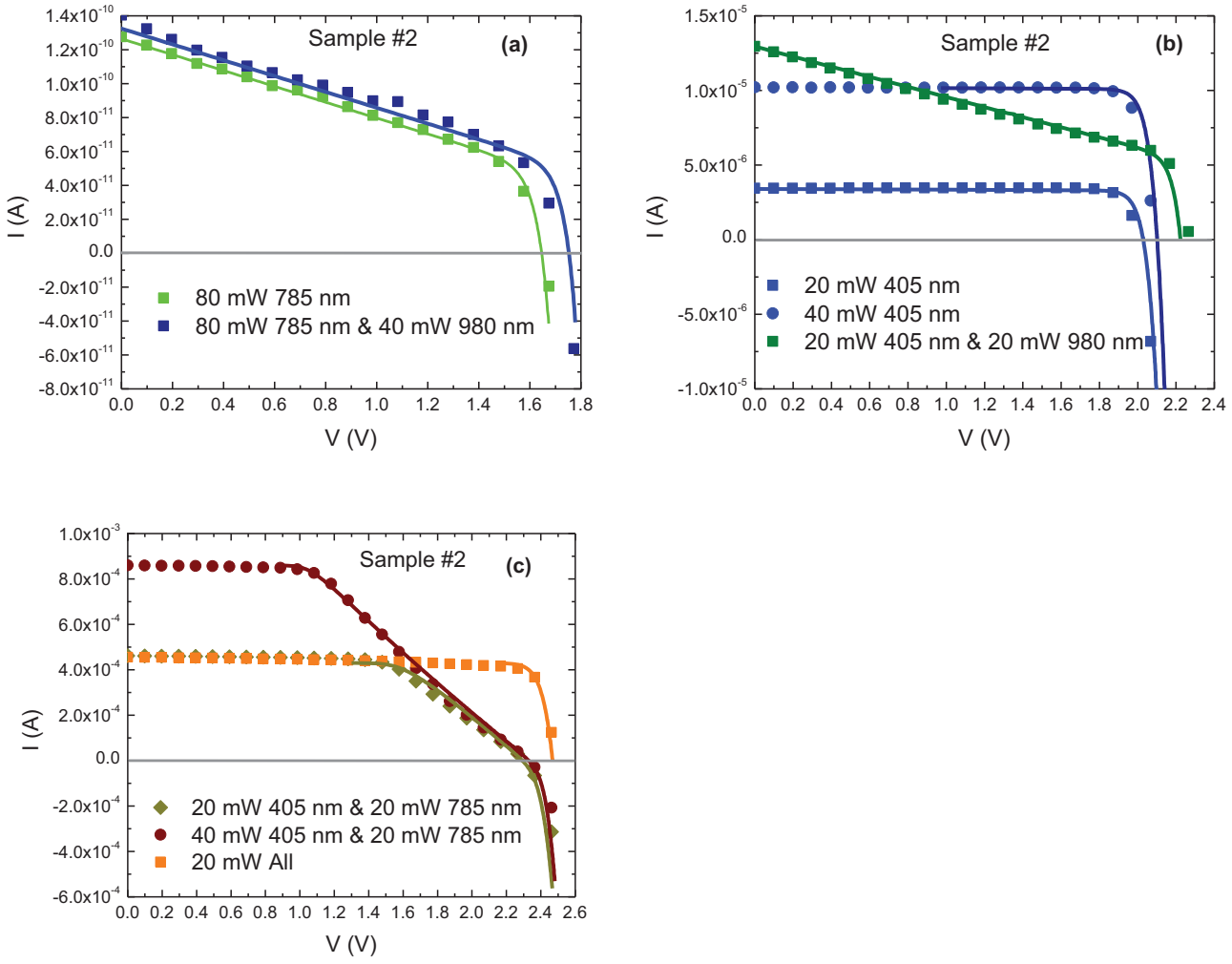

Fig. B1. $I(V)$ experimental results (symbols) obtained on the second sample. The power of the lasers used for the experiment is displayed in the figure. The lines are the fits obtained with the numerical simulation.

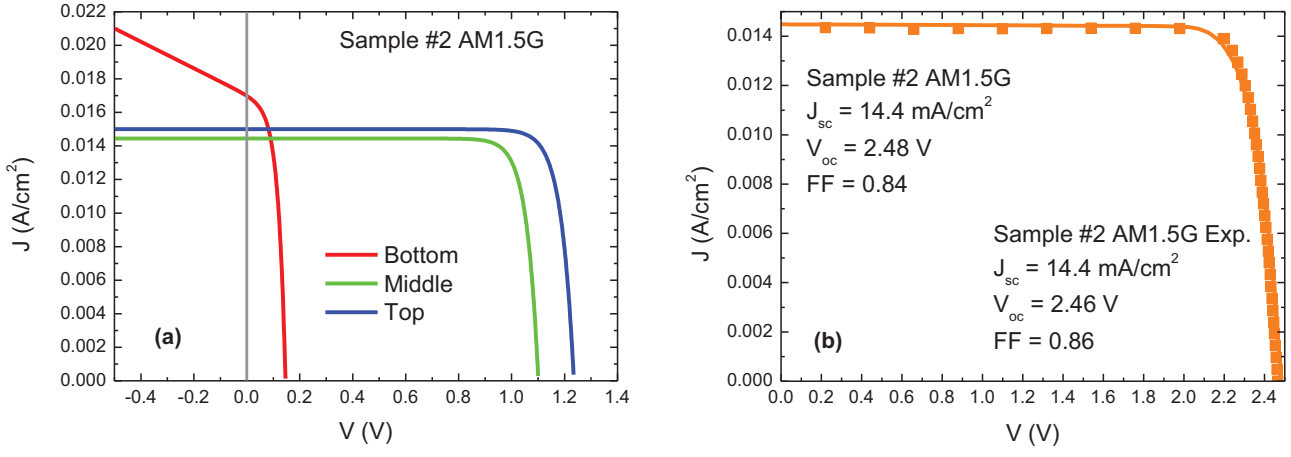

Fig. B2. (a) $J(V)$ characteristics of each junction of sample #2 taken alone under AM1.5G, (b) comparison of the experimental (squares) and theoretical (line) $J(V)$ characteristics of the device under AM1.5G.

Author contribution statement

All the authors contributed equally to this work.

References

1. F. Dimroth, T.N.D. Tibbits, M. Niemeyer et al., IEEE J. Photovolt **6**, 343 (2016)
2. A.J.K. Leoga, A. Ritou, M. Blanchard et al., arXiv: 2301.07079 (2023)
3. C. Domínguez, N. Jost, S. Askins, M. Victoria, I. Antón, Proc. AIP Conf. **1881**, 080003 (2017)
4. N. Hayashi et al., Proc. AIP Conf. **1881**, 080005 (2017)
5. N. Jost, G. Vallerotto, A. Tripoli, S. Askins, C. Domínguez, I. Antón, Sol. Energy Mater. Sol. Cells **245**, 111882 (2022)
6. A. Ritou, P. Voarino, O. Raccurt, Sol. Energy **173**, 789 (2018)
7. M. Wiesenfarth, M. Steiner, H. Helmers, A.W. Bett, Sol. Energy Mater. Sol. Cells **219**, 110791 (2021)
8. M. Wiesenfarth et al., Proc. AIP Conf. **2550**, 030008 (2022)
9. P. Albert et al., Prog. Photovolt.: Res. Appl. **29**, 990 (2021)
10. M. de Lafontaine et al., Micro Nano Eng. **11**, 100083 (2021)
11. M. de Lafontaine et al., Sol. Energy Mater. Sol. Cells **239**, 111643 (2022)
12. J. Burdick, T. Glatfelter, Sol. Cells **18**, 301 (1986)
13. M. Meusel, C. Baur, G. Létay, A.W. Bett, W. Warta, E. Fernandez, Prog. Photovolt.: Res. Appl. **11**, 499 (2003)
14. S. Fafard, C.E. Valdivia, S.G. Wallace, Proc. AIP Conf. **1477**, 118 (2012)
15. V. Paraskeva, M. Hadjipanayi, M. Norton, M. Pravettoni, G.E. Georghiou, Sol. Energy Mater. Sol. Cells **116**, 55 (2013)
16. G. Siefer, C. Baur, A.W. Bett, in *Proceedings of the 2010 35th IEEE Photovoltaic Specialists Conference* (2010), p. 000704
17. J.F. Geisz, W.E. MacMahon, J. Buencuerpo, M.S. Young, M. Rienäcker, A. Tamboli, E.L. Warren, Cell Rep. Phys. Sci. **2**, 100677 (2021)
18. This software is available at https://www.geeps.centralesupelec.fr/index.php?page=logiciel-triple_junction
19. O. Breitenstein, J.P. Rakotoniaina, M.H. Al Rifai, M. Werner, Prog. Photovolt.: Res. Appl. **12**, 529 (2004)
20. J.M. Gordon, E.A. Katz, W. Tassew, D. Feuermann, Appl. Phys. Lett. **86**, 073508 (2005)
21. T.B. Stellwag et al., in *Proceedings of the IEEE Conference on Photovoltaic Specialists* (1990), p. 442
22. O. Breitenstein, P. Altermatt, K. Ramspeck, A. Schenk, in *Proceedings of the 21st European Photovoltaic Solar Energy Conference* (WIP Renewable energies, 2006), pp. 625–628
23. R.R. King, D. Bhusari, A. Boca, D. Larrabee, X.-Q. Liu, W. Hong, C.M. Fetzer, D.C. Law, N.H. Karam, Prog. Photovolt. **19**, 797 (2011)

Citation de l'article : Christophe Longeaud, José Alvarez, Herinirina Fanevamampiandra, Thomas Bidaud, Gwenaëlle Hamon, Maxime Darnon, Marie-Estelle Gueunier-Farret, Determination of individual $I(V)$ characteristics of each sub-cell of a triple junction device, EPJ Photovoltaics 14, 20 (2023)